Received: 1 September 2020 | Revised: 4 January 2021 | Accepted: 5 January 2021

DOI: 10.1002/mrm.28700

RAPID COMMUNICATION

Magnetic Resonance in Medicine

Deuterated water imaging of the rat brain following metabolism of [$^2H_7$]glucose

Rohit Mahar[1] | **Huadong Zeng**[2] | **Anthony Giacalone**[1] | **Mukundan Ragavan**[1] | **Thomas H. Mareci**[1] | **Matthew E. Merritt**[1]

[1]Department of Biochemistry and Molecular Biology, College of Medicine, University of Florida, Gainesville, Florida, USA

[2]Advanced Magnetic Resonance Imaging and Spectroscopy Facility, College of Medicine, University of Florida, Gainesville, Florida, USA

Correspondence
Matthew E. Merritt, Department of Biochemistry and Molecular Biology, College of Medicine, University of Florida, Gainesville, FL 32610, USA.
Email: matthewmerritt@ufl.edu

Funding information
National Science Foundation, Grant/Award Number: DMR-1644779; National Institutes of Health, Grant/Award Number: 5U2C-DK119889, P41-122698 and R01-DK105346

Purpose: To determine whether deuterated water (HDO) generated from the metabolism of [$^2H_7$]glucose is a sensitive biomarker of cerebral glycolysis and oxidative flux.

Methods: A bolus of [$^2H_7$]glucose was injected through the tail vein at 1.95 g/kg into Sprague-Dawley rats. A ^2H surface coil was placed on top of the head to record ^2H spectra of the brain every 1.3 minutes to measure glucose uptake and metabolism to HDO, lactate, and glutamate/glutamine. A two-point Dixon method based on a gradient-echo sequence was used to reconstruct deuterated glucose and water (HDO) images selectively.

Results: The background HDO signal could be detected and imaged before glucose injection. The ^2H NMR spectra showed arrival of [$^2H_7$]glucose and its metabolism in a time-dependent manner. A ratio of the HDO to glutamate/glutamine resonances demonstrates a pseudo–steady state following injection, in which cerebral metabolism dominates wash-in of HDO generated by peripheral metabolism. Brain spectroscopy reveals that HDO generation is linear with lactate and glutamate/glutamine appearance in the appropriate pseudo–steady state window. Selective imaging of HDO and glucose is easily accomplished using a gradient-echo method.

Conclusion: Metabolic imaging of HDO, as a marker of glucose, lactate, and glutamate/glutamine metabolism, has been shown here for the first time. Cerebral glucose metabolism can be assessed efficiently using a standard gradient-echo sequence that provides superior in-plane resolution compared with CSI-based techniques.

KEYWORDS
[$^2H_7$]glucose, brain, DMRI, HDO, metabolism

1 | INTRODUCTION

Glucose is the principal source of energy in the brain, and its dynamic uptake and use remain a key topic after decades of research. Metabolic imaging using MR-based methods has traditionally been limited to ^1H-based spectroscopic detection of metabolites through CSI or single-voxel spectroscopy.[1,2] Although these methods have been of immense

use in clinical research, sensitivity issues have made their translation to the clinic problematic. More recently, hyperpolarized ^{13}C imaging has been used to study heart, liver, and brain metabolism, as well as changes in metabolism associated with various cancers.[3,4] Hyperpolarized imaging uses the large gain in SNR made possible by dynamic nuclear polarization to produce chemically selective images that reflect changes in metabolic flux.[5] However, dynamic nuclear polarization is limited to molecules having long relaxation times amenable to sample transfer from the polarizer to the patient. Many important metabolites such as glucose have short relaxation times, making clinical translation more challenging.[6] 2-[^{18}F]fluorodeoxyglucose (FDG) PET is used widely for cancer diagnosis, staging, and treatment assessment.[7] However, the specificity of FDG-PET is limited in the brain, where normally high glucose uptake and noncancerous inflammation can give false positive results.[8] Additionally, FDG-PET is limited to glucose uptake and phosphorylation; glycolytic and tricarboxylic acid (TCA) cycle metabolism are invisible to this technique.

Another approach that uses the chemical selectivity of MR uses ^{2}H-labeled substrates to image metabolic turnover. Lu et al demonstrated in vivo deuterium MRS using [6,6-$^2H_2$] glucose to measure glucose uptake and glutamate/glutamine (glx) production over time, providing an alternative method for turnover studies in the brain.[9] In a seminal publication, the same glucose isotopomer was used to image human glioblastoma.[10] However, the deuterated glucose isotopomer chosen for the study predetermined that downstream deuteration at lactate-C3 and glx-C4 would necessarily be the metabolic readouts of glucose metabolism. These peaks are slowly enriched as a function of time, and are most easily imaged using the CSI technique, as they are smaller peaks relative to the deuterated water (HDO) signal that arises both from natural abundance contributions and from a limited set of exchange reactions that eliminate the ^{2}H label from the methyl position of lactate. We recently proposed [$^2H_7$]glucose as an alternative agent, and showed in cell culture that HDO evolution accurately reflected total glucose uptake,[11] in analogy to FDG-PET,[12] but with detection of glucose downstream metabolism and without the use of ionizing radiation.

Here we demonstrate the application of this method in vivo to image glucose consumption in the rat brain. Administration of [$^2H_7$]glucose through the tail vein produced deuterated lactate and glx analogous to earlier reports, but here we show for the first time that HDO generated from metabolism can be imaged in the rodent brain using gradient echo–based methods as opposed to CSI. Using methods other than CSI to detect metabolic flux fundamentally transforms the technique, allowing excellent in-plane resolution and faster acquisition times. Using HDO evolution as a metric of glucose use in the brain, we introduce a biomarker of cerebral glycolysis and oxidative flux that is imaged with superior sensitivity and resolution compared with previous approaches.

2 | METHODS

2.1 | Chemicals and tracer

[1,2,3,4,5,6,6-$^2H_7$]-D-glucose (or [$^2H_7$]glucose) was purchased from Sigma-Aldrich (St. Louis, MO). Isoflurane anesthesia was purchased from Aspen Veterinary Resources (Liberty, MO). Sterile filtered saline solution was prepared to dissolve the [$^2H_7$]glucose solution. Heparin at 1000 USP/mL of glucose solution was also used to stop the clotting of blood during animal preparation.

2.2 | Animal experimental setup

All experimental procedures were approved by the University of Florida Institutional Animal Care and Use Committee. Female Sprague-Dawley rats (body weight ~220 g) were purchased from Jackson Laboratory (Bar Harbor, ME) and acclimatized in the University's animal care facilities. All rats were in the fed state. The rat was anesthetized with 2% isoflurane in a mixture of O_2 and N_2 gases. The tail vein was catheterized using a 23-gauge needle for the infusion of [$^2H_7$]glucose tracer. The body temperature of the rat was maintained at 37ºC using a heated circulating water pad. The respiratory rate was monitored during the entire period of the experiment. After shimming the magnet, three baseline ^{2}H spectra were acquired. Subsequently, a 2-minute tail vein infusion of [$^2H_7$]glucose (1.95 g/kg body weight and dissolved in 2.3 mL saline) was administered. Blood was drawn after the end of spectroscopy and imaging experiments through the saphenous vein, and blood plasma was separated by centrifugation of the blood at 4ºC for 10 minutes. Circulating blood glucose was assessed by a blood draw and glucometer (Evancare; Medline Industries, Northfield, IL) before infusion and 3 hours after the glucose injection.

2.3 | Magnetic resonance imaging system

Animal experiments were performed on an 11.1 T Magnex magnet (Magnex Scientific, Yarnton, United Kingdom) interfaced to a Bruker Avance III HD console running on *ParaVision* 6.0.1 (Bruker Biospin, Billerica, MA). The MRI system was equipped with RRI BFG-240/120-S6 gradient coil with the bore size of 120 mm and capable of producing 100 mT/m with 200-μs rise time. A shim map was generated for localized shimming on rat brain using an 85-mm home-built, actively decoupled, linear-volume

^{1}H transmit-receive coil. The coil was tuned to the ^{1}H-NMR frequency at 470 MHz. A home-built 14-mm diameter, circular surface coil tuned to 72.26 MHz was used to acquire ^{2}H spectra and images.

2.4 | Deuterium MRS

The ^{2}H coil was placed over the rat head, and a 3D-printed phantom containing approximately 200 μL of natural abundance water was placed on the top of the coil to confirm positioning. The ^{2}H-RF pulse and flip angle were optimized to maximize the ^{2}H signals from the rat brain. A partial signal contribution from the natural abundance ^{2}H of the water phantom was unavoidable but was accounted for by subtraction of the signal areas from runs that followed the glucose injection. A single pulse–acquire sequence was used to obtain ^{2}H-NMR spectra, with an observed linewidth of about 40 Hz. Spectra were acquired with a 1 kHz spectral width and 256 data points for each FID, a TR of 300 ms, and a flip angle of 60º with 256 averages. The total acquisition time for each spectrum was 1.28 minutes. A total of 30 spectra were acquired for a 38-minute time period. Two additional ^{2}H-NMR spectra from the rat brain were acquired at 2 hours and 2.5 hours following [$^{2}H_7$]glucose infusion. Pyrazine-D_4 (2.5 mM, internal standard) was added in each plasma sample to calculate the HDO concentration in plasma. The ^{2}H-NMR spectra were collected on a Bruker 14 T NMR magnet system equipped with a 1.7 mm TCI CryoProbe and Avance Neo console (Bruker BioSpin). The ^{2}H-NMR spectra of plasma samples were acquired at 92.13 MHz resonant frequency with an acquisition time of 1.0 second, relaxation delay of 2 seconds, and 3072 scans.

2.5 | Deuterium MRI

Axial ^{1}H images of rat brain were acquired using a Bruker FLASH gradient-echo sequence. The 2D acquisition matrix size of 128 × 128, FOV of 50 × 50 mm^2, and eight averages were used to acquire 10 slices of rat brain with 2-mm thickness. Before [$^{2}H_7$]glucose infusion, a natural abundance deuterium ^{2}H image of the rat brain was acquired using the FLASH sequence, with the ^{2}H water signal on resonance. Two deuterium images were also acquired at 38 minutes and about 2 hours following [$^{2}H_7$]glucose infusion. The following parameters were used to acquire axial ^{2}H images of the rat brain: 2D acquisition matrix size = 32 × 32, FOV = 50 × 50 mm^2, slice thickness = 14 mm, TR = 100 ms, 256 signal averages, 1.416 ms TE, and 34.2º flip angle with an in-plane resolution of 1.56 mm^2. Each image took 13 minutes to acquire. The Bruker multigradient-echo (MGE) imaging experiment was used to acquire the echo images for separating HDO-only and [$^{2}H_7$]glucose-only images in the rat brain during the pseudo–steady state. Axial two-echo images were acquired with TEs of 11.1 ms (GE1) and 16.6 ms (GE2), acquisition matrix size of 32 × 32, FOV of 40 × 40 mm^2, and slice thickness of 14 mm. The in-plane resolution was 1.25 mm^2. Proton intensity images of the rat brain was also acquired with the same FOV as deuterium images for co-registration purposes.

2.6 | Nuclear magnetic resonance and MRI data processing

The ^{2}H-NMR data analysis was performed using *MestReNova* version 14.0.1-23284 (Mestrelab Research, Santiago, Spain). For processing of the ^{2}H NMR, each spectrum was Fourier transformed with an exponential window function of 2.0 Hz, zero-filling of 512 data points, and automatic phase correction was also applied. Peak areas were extracted for HDO, [$^{2}H_7$]glucose including the anomeric signal, deuterated glx, and lactate from the ^{2}H-NMR spectra of the rat brain. Two-dimensional ^{1}H and ^{2}H images were processed in the *ImageJ* software (National Institutes of Health, Bethesda, MD). Because the acquired ^{2}H image size was 32 × 32 and the ^{1}H brain image was 128 × 128, the deuterium image was scaled using bicubic interpolation to 128 × 128 for co-registration and overlay of the images. This resulted in a final, interpolated, in-plane resolution of 0.39 mm^2. The MGE echo images were reconstructed to 128 × 128 matrix size with Gaussian windowing filter using Bruker *ParaVision* 6.0.1 software. Reconstructed echo images were imported to *MATLAB* (MathWorks, Natick, MA) for further processing, to separate the contribution of HDO and [$^{2}H_7$]glucose to the rat brain deuterium MRI. The Dixon reconstruction algorithm[13] was applied to reconstruct the HDO-only and [$^{2}H_7$]glucose-only images from the MGE images. T_2 relaxation times of HDO and [$^{2}H_7$]glucose were also used as part of the Dixon reconstruction.[14]

3 | RESULTS

The initial blood glucose was measured as 8.0 ± 1.4 mM (N = 4) before infusion, and the final blood glucose concentration at 3 hours after injection was 7.1 ± 1.8 mM (N = 4). The natural-abundance HDO water signal (Figure 1A) obtained using a surface coil with the 200 μL phantom in place is assumed to reflect the 0.015% enrichment of HDO in water (~13.2 mM, assuming the brain is 75% water by mass, and accounting for the phantom). The subsequent panels show the arrival of a bolus of [$^{2}H_7$]glucose and its metabolism to glx and lactate (Figure 1C, D). Over the course of 2.5 hours, the glucose bolus is almost completely metabolized,

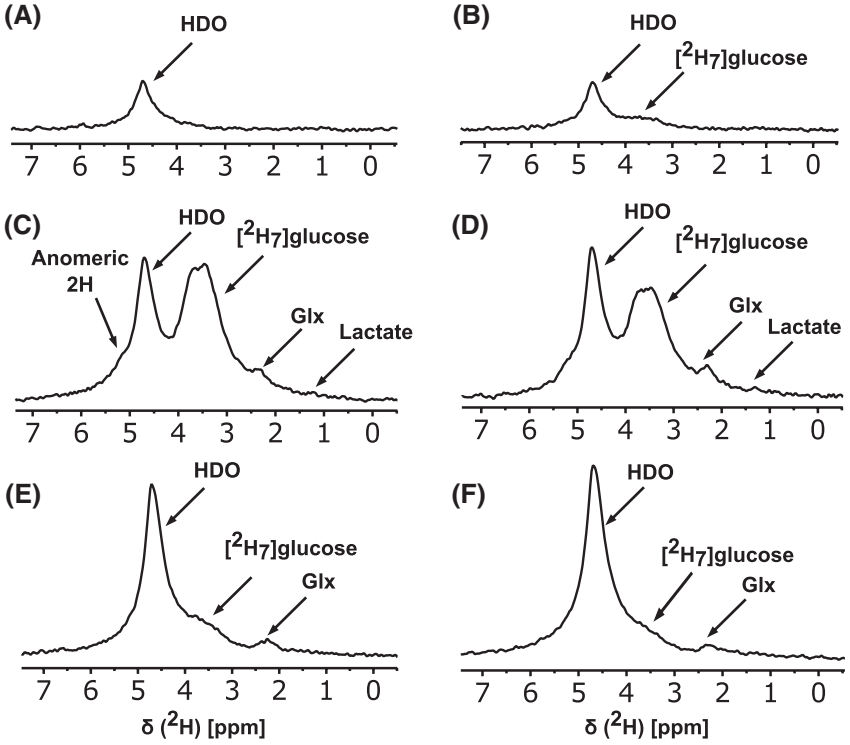

FIGURE 1 Representative time-series ^{2}H-NMR spectra obtained from rat brain. The ^{2}H-NMR spectra represent natural-abundance deuterium signal before [$^2H_7$]glucose infusion (A), 2 minutes after infusion (B), 24 minutes after infusion (C), 35 minutes after infusion (D), 120 minutes after infusion (E), and 150 minutes after [$^2H_7$]glucose infusion (F). Each in vivo ^{2}H-NMR spectrum was obtained from a single 256-scan acquisition. The ^{2}H resonance assignments are for deuterated water (HDO), [$^2H_7$]glucose including the anomeric deuterium, deuterated glutamate/glutamine (glx), and deuterated lactate

returning to a level just above the detection limit (Figure 1F). Most importantly, the HDO signal increased rapidly initially, then continued to rise at a slower rate as metabolism continues (Figure 2). At the end of the experiment, the HDO signal dominates both the residual glucose and the remaining glx signal (Figure 1F). The kinetics of the deuterated precursor and products includes the HDO signal after a correction for the natural-abundance HDO (Figure 2). The lactate and glx signals display similar kinetics, rising with increasing glucose concentration, then slowly decreasing, albeit at a slower rate than the glucose signal. It should be noted that turnover of the lactate and glx pools could continue to contribute to the HDO pool size. At longer time points (Figure 2B), the HDO signal does not fall, but continues to increase to a final estimated concentration approximately 3.5 times greater than the natural abundance signal, corresponding to ~48 ± 10 mM ($N = 3$). A plot of the HDO signal intensity versus the glucose consumption showed a bimodal response following the initial arrival of the glucose tracer (Supporting information Figure S1). HDO intensity was plotted as a ratio against glx and lactate intensities as a means of assessing the correlation between HDO production, LDH flux, and TCA cycle activity (Figure 2C). After the initial appearance of the metabolites, a pseudo–steady state for the ratios is reached in the range of 10-24 minutes.

Two gradient-echo images were acquired at about 38 minutes and 2 hours following infusion. The initial image before injection shows a very faint background HDO signal, which increases significantly with time (Figure 3F, I) after injection of [$^2H_7$]glucose. The improved SNR allows a rudimentary coil-sensitivity profile to be visualized. The image shown in Figure 3E was acquired with HDO on resonance, beginning at 38 minutes following infusion, but it is subject to a significant chemical shift artifact associated with the glucose signal. At 2.5 hours after infusion, the HDO is by far the largest signal, and does not have a significant contribution from the glucose signal.

To distinguish the HDO signal from the [$^2H_7$]glucose substrate, an MGE-based two-point Dixon method was implemented during the initial time period (~10-24 minutes) of the post-[$^2H_7$]glucose infusion and metabolism (Figure 4). Figure 4D,F shows the HDO-only and [$^2H_7$]glucose-only images, respectively. Blood plasma collected at the end of the experiment was used to assess the final body water HDO enrichment, which was determined to be 86.9 ± 5.16 mM ($N = 4$).

4 | DISCUSSION

The brain image in Figure 3 is the first demonstration of the efficacious use of HDO generated from [$^2H_7$]glucose as a means for producing metabolically sensitive MR images using simple gradient-echo methods.[15] By choosing the metabolic product HDO as the target, drawbacks associated with imaging relatively low-concentration metabolites, like lactate and glx, are bypassed. Metabolism of [$^2H_7$]glucose can produce HDO through flux into the 3-carbon glycolytic intermediates, and through oxidation of the downstream deuterated acetyl-CoA (Figure 5). It can also be produced by multiple enzyme-catalyzed exchange reactions like, for example, triose phosphate isomerase[16,17]

and alanine aminotransferase.[18] The HDO production from the C1/C2 positions of fructose-6-phosphate and mannose-6-phosphate can also occur through phosphomannoseisomerase.[19] In this case, we neglect the possible action of the pentose phosphate pathway. Of the possible HDO-generating processes, only the keto-enol tautomerization[20] is purely chemical in nature. Previous work suggests that it could account for a maximum of 8% of the HDO generation when using [6,6-$^2H_2$]glucose,[10] indicating that its contribution in this case should be very small in relative terms. In our recent work in Huh-7 cancer cells incubated with [$^2H_7$]glucose, we observed that unlabeled lactate

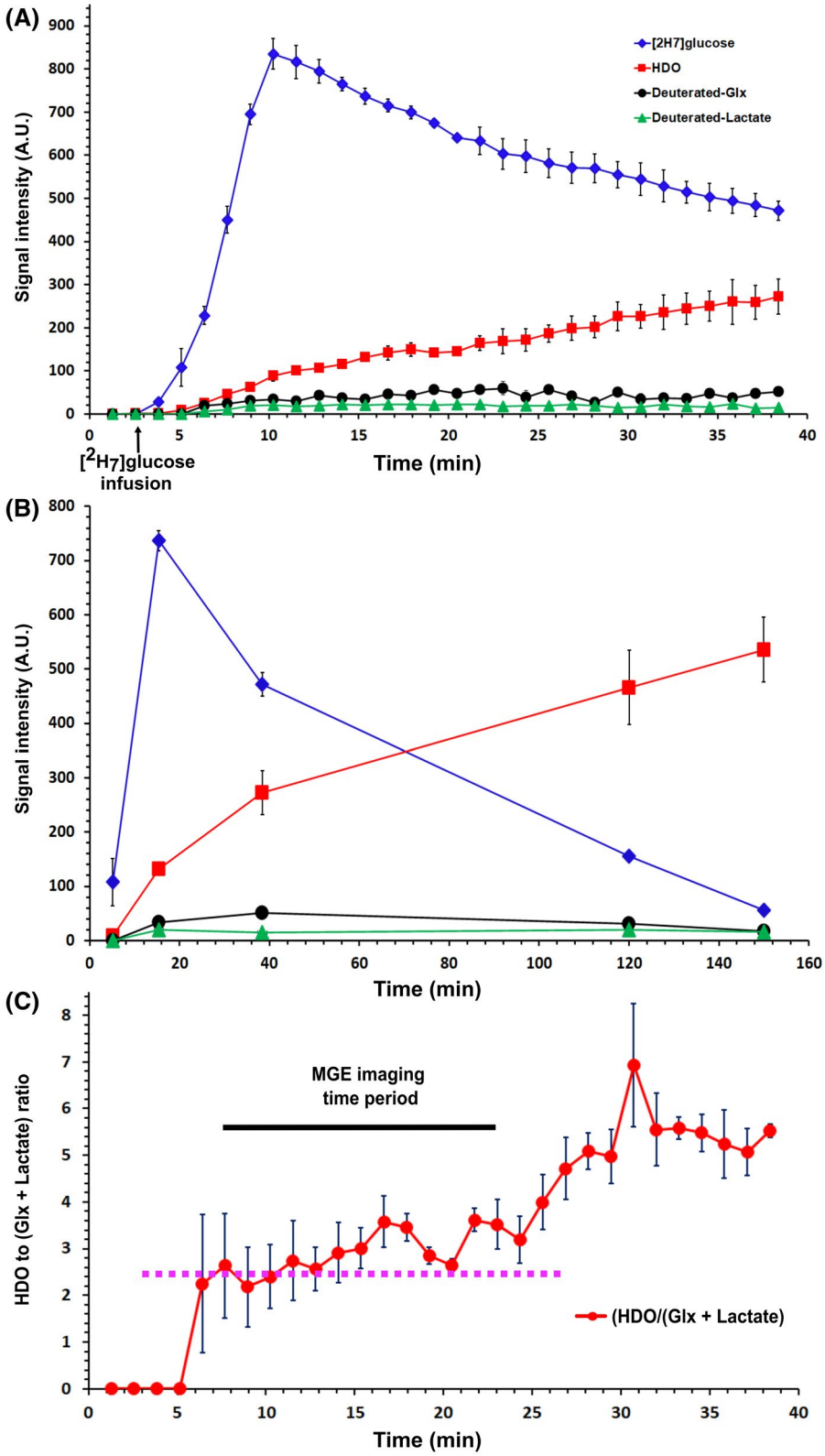

FIGURE 2 The time series for the signals of [$^2H_7$]glucose, HDO, glx, and lactate was calculated using the fitted areas for the ^{2}H-MRS data from rat brain. A, A series of data points indicating the absorption and use of [$^2H_7$]glucose for production of HDO, deuterated glx, and deuterated lactate. [$^2H_7$]glucose (blue diamonds) increases in signal intensity on delivery and subsequently decreases in its signal intensity with time. The HDO (red squares) shows a continuous increase in the signal intensity following [$^2H_7$]glucose infusion. The glx (black circles) and deuterated lactate (green triangles) show an increase in the signal intensity and slight decrease at the end of the experiment. B, The five time points (5 minutes, 15 minutes, 38 minutes, 2 hours, and 2.5 hours) of the dynamic change in the signals of [$^2H_7$]glucose, HDO, deuterated glx, and deuterated lactate. The HDO (red diamonds) concentration continuously increased with time, even after the cerebral glucose was apparently consumed. Body water enrichment of HDO was approximately 1.8 times greater than the brain concentration at the final time point, indicating that the continual increase was likely due to continued glx and lactate turnover, as well as extracerebral metabolism. The plot in panel (C) shows the ratio HDO to lactate+glx (red line) as a function of time. This ratio is stable from ~8 to 24 minutes. Note: The natural-abundance deuterated HDO signal intensity was subtracted from the HDO signal of each spectrum. Data are represented as mean ± SEM. Abbreviation: MGE, multigradient echo

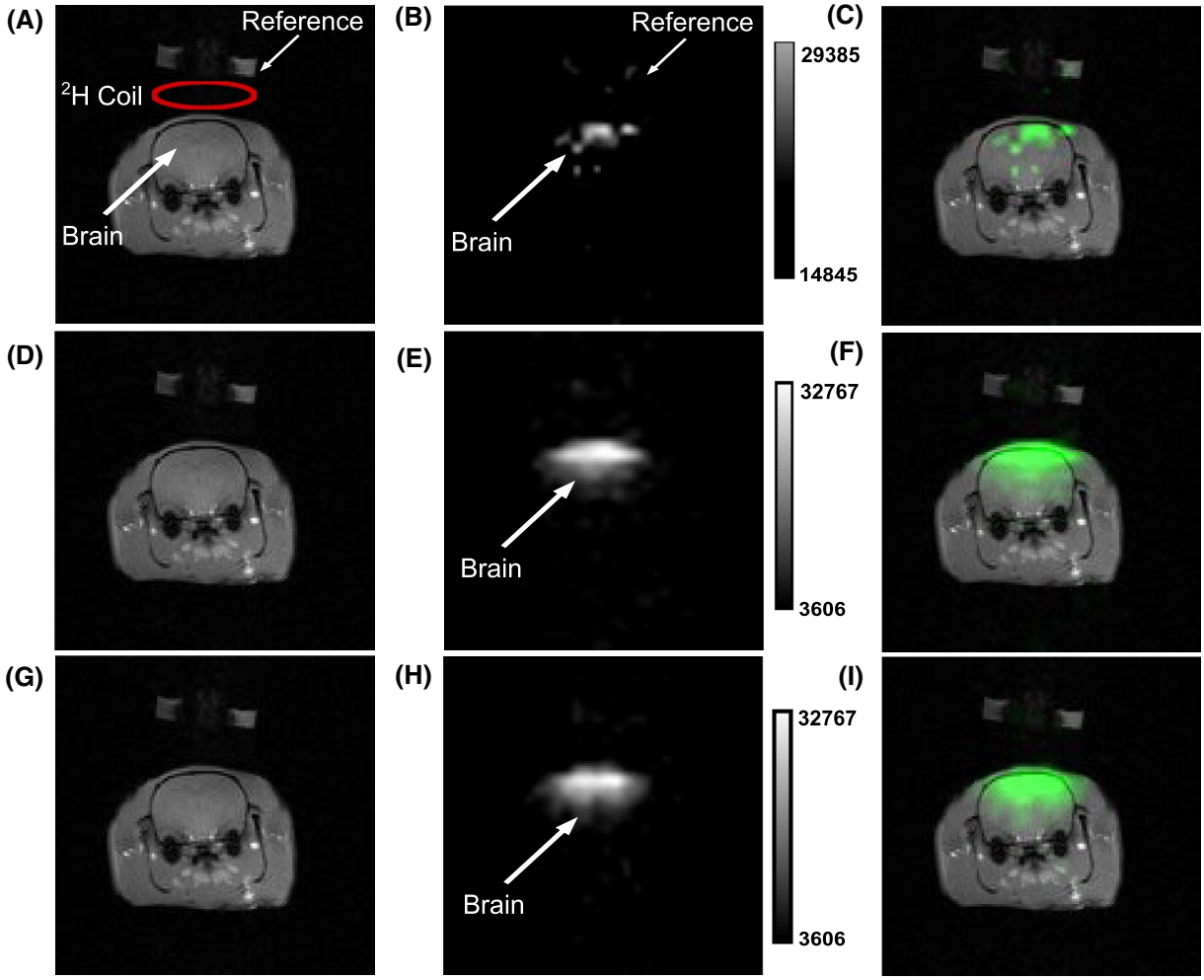

FIGURE 3 Deuterium MRI images show the consumption of [$^2H_7$]glucose and production of HDO in the brain. A, Proton intensity image of brain and a container for tap water as a reference for deuterium surface coil positioning. B, Natural-abundance deuterium pre-[$^2H_7$]glucose infusion. C, Overlaid image of the proton (gray) (A) and deuterium (green) (B) image. E, Deuterium intensity image after 50 minutes of [$^2H_7$] glucose infusion. F, Overlaid images of proton (gray) (D) and deuterium (green) (E) intensity images. H, Deuterium image after 2.5 hours of the [$^2H_7$]glucose infusion. I, Overlaid images of proton (gray) (G) and deuterium (green) (H) intensity images. Note: Parts (A), (D), and (G) are proton intensity images obtained before every corresponding deuterium image for co-registration of proton and deuterium images. Size of deuterium images was scaled by interpolation to the proton image for co-registration of the images

increased with time, suggesting significant deuterium loss during glycolysis.[11] The stoichiometry of the metabolism of the deuterated tracer is such that the number of HDO molecules produced by glycolysis versus glx and lactate ^{2}H enrichment varies depending upon whether the glycolytically derived pyruvate methyl group is produced from either the C1 or C6 position of glucose (Figure 5). Multiple reactions, including equilibration at M6P, alanine, or

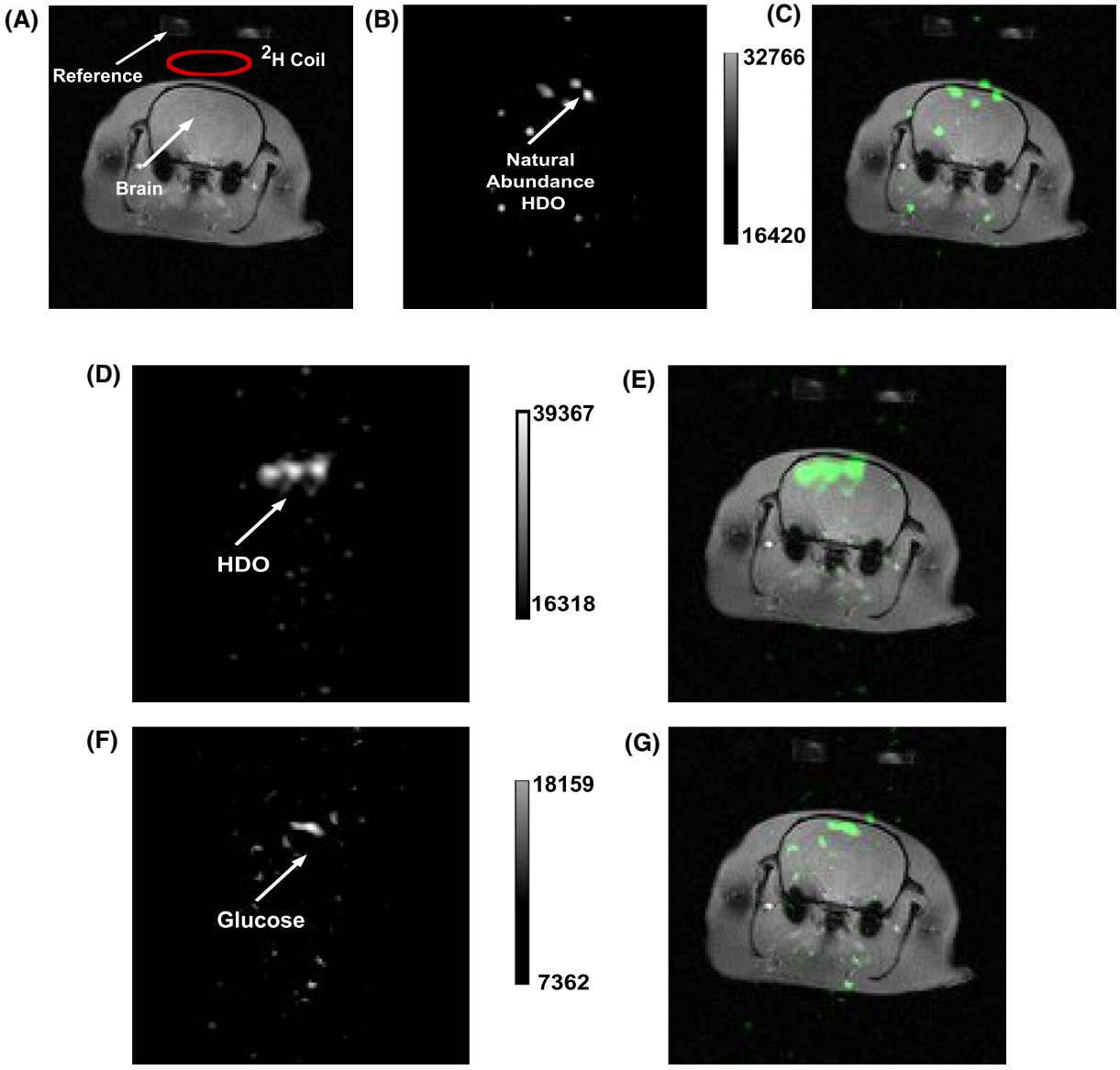

FIGURE 4 Multigradient-echo imaging separates the contribution of [$^2H_7$]glucose and HDO to deuterium MRI of the rat brain. A, Proton intensity image of brain. B, Natural-abundance HDO pre-[$^2H_7$]glucose infusion image. C, Overlaid image of the proton (gray) (A) and deuterium (green) (B) images. D, Deuterium image of HDO only. E, Overlaid images of proton (gray) (A) and deuterium (green) (D) images due to HDO only in the rat brain. F, Deuterium image from the contribution of [$^2H_7$]glucose only. G, Overlaid image of proton (gray) (A) and deuterium (green) (F) [$^2H_7$]glucose-only images

pyruvate keto-enol tautomerization, can result in a singly deuterated or completely protonated pyruvate entering the TCA cycle (Supporting information, Figure S2). If we assume that cerebral glucose produces either lactate or glx, and that deuterium can be lost to exchange at either the C1 or the C6 position, the theoretical yield of pyruvate isotopomers should produce a total HDO/(glx + lactate) ratio of 20/8 or 2.5. Recent work by de Graaf addresses the effects of exchange directly using rodent brain extracts at time points equivalent to those used here.[21] Our data was corrected with their measured deuterium depletion, including the fraction of pyruvate that has no deuterium atoms left after glycolysis, to produce Figure 2C. Note that due to the action of isocitrate dehydrogenase, deuterium should be totally eliminated from TCA cycle intermediates on the second turn of the cycle, implying that glx enrichment is due to "first pass" kinetics only. Therefore, the HDO/(glx + lactate) value of 2.5 should be robustly conserved in normal tissue. This value is illustrated as the dotted line in Figure 2C, and the experimentally determined ratio closely conforms to this value for approximately 15 minutes after the maximal circulating glucose concentration in the brain is achieved ($N = 3$). After this time period, HDO continues to rise more rapidly than lactate and glx. We attribute the increasing HDO signal in the brain late after injection to the influx of HDO generated by glucose metabolism in

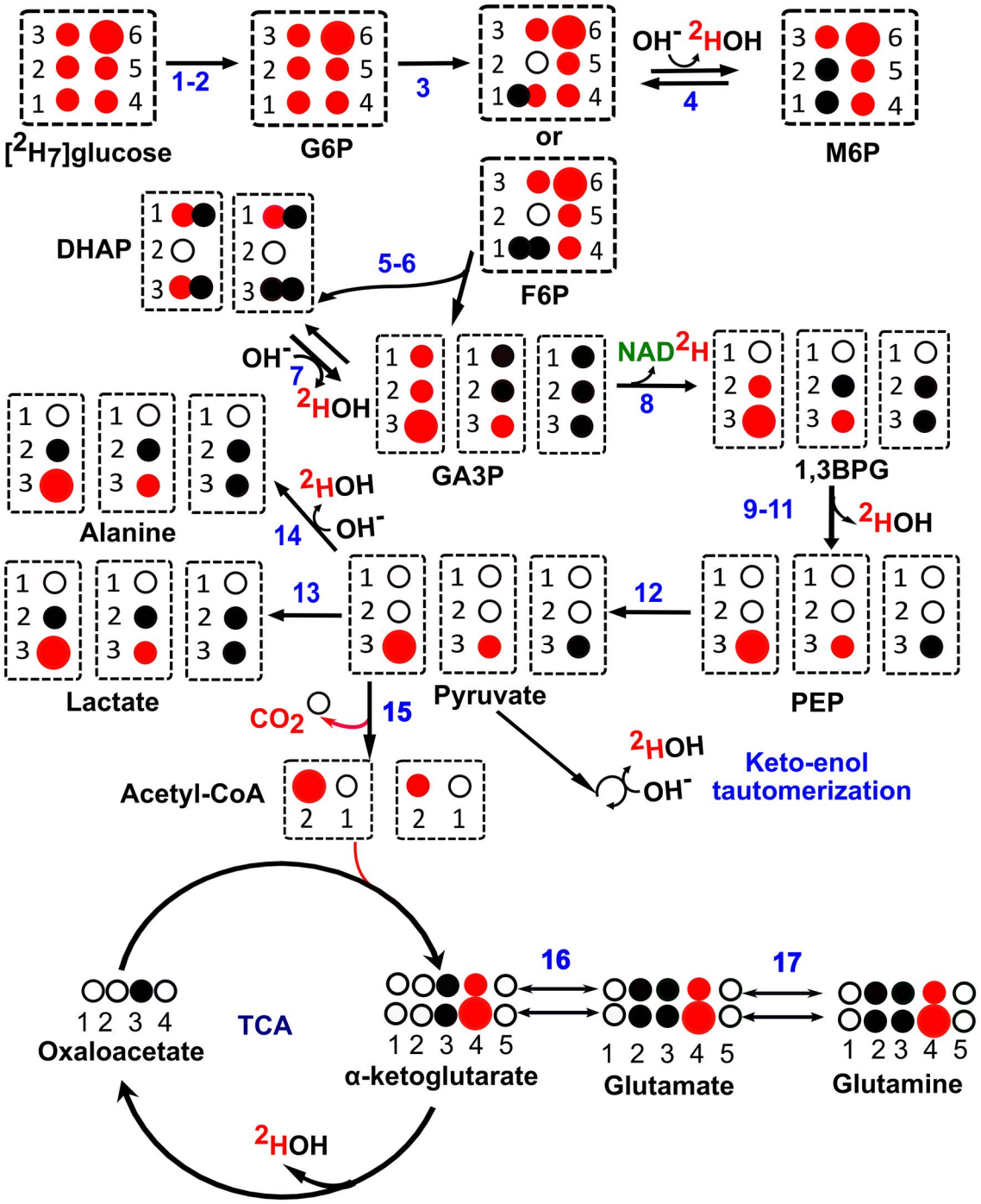

FIGURE 5 Schematic representation of the production of deuterated lactate, glx, and HDO from [$^2H_7$]glucose during glycolysis and the tricarboxylic acid (TCA) cycle. Deuterium (^2H) loss has been shown in the form of ^{2}HOH and NAD^{2}H. Small and large red-filled circles represent one and two deuterium atoms, respectively, and black-filled and empty circles represent hydrogen atoms and quaternary carbons, respectively. Enzymes involved in glycolysis and TCA cycle are as follows: (1) hexokinase (HK), (2) glucokinase (GK), (3) glucose-6-phosphate isomerase (GPI), (4) phosphomannoseisomerase (PMI), (5) phosphofructokinase (PFK), (6) fructose bisphosphate aldolase (FBPA or aldolase), (7) triose phosphate isomerase (TPI), (8) glyceraldehyde phosphate dehydrogenase (GAPDH), (9) phosphoglycerate kinase (PGK), (10) phosphoglyceromutase (PGM), (11) enolase, (12) pyruvate kinase (PK), (13) lactate dehydrogenase (LDH), (14) alanine aminotransferase (ALT), (15) pyruvate dehydrogenase (PDH), (16) glutamate dehydrogenase (GDH), and (17) glutamine synthetase (GS). Note: Unlabeled lactate, pyruvate, glutamate, and glutamine can be produced due to deuterium loss from the deuterated precursors in glycolysis and by multiple turns of the TCA cycle. Abbreviations: G6P, glucose-6-phosphate; F6P, fructose-6-phosphate; M6P, mannose-6-phosphate; DHAP, dihydroxy acetone phosphate; GA3P, glyceraldehyde 3-phosphate; PEP, phospho-enol pyruvate

peripheral tissues, or to "second pass" TCA cycle turnover generating additional HDO. These data strongly suggest that imaging HDO during the time period of 10-24 minutes is equivalent to estimates of lactate and glx kinetics, albeit with significantly higher sensitivity. This time period was used when we applied the HDO/glucose two-point Dixon imaging (Figure 4).

As detailed in the results, the first ^{2}H image after glucose injection (Figure 3E) is a convolution of the HDO and glucose signals. These images were of sufficient SNR to allow us to implement frequency-selective imaging. We have optimized an MGE two-point Dixon method to produce HDO-versus-glucose images (Figure 4D, F) in analogy to fat–water imaging.[22] The in-plane resolution was reduced to 1.25 mm^2 in these images, based only on the imaging parameters before data processing. Chemical shift imaging could not produce images of this resolution even at time periods about 4 times as long for acquisition. Increasing imaging specificity could be encoded using multipoint Dixon methods to account for glx and lactate signals,[23] but this approach was not implemented for this study. We have treated the maximal glucose intensity at about 3.4 ppm as the center of the glucose signal. This is obviously a compromise to maintain the simplicity of the imaging method. Phase dispersion associated with the inhomogeneously broadened glucose signal likely costs sensitivity in the reconstructed glucose image of Figure 4F. We believe the HDO signal is largely free from these issues, although a small component originating from the anomeric deuterium of glucose is also present under the HDO signal. In total, the HDO image should serve as an accurate biomarker of glycolytic flux. The HDO image should also recapitulate glx kinetics in the case of normally functioning brain tissue. The HDO image would fail to report on TCA cycle kinetics in the case of a Warburg phenotype.

Although the images here were acquired with a significant slice thickness that must cause significant partial-volume effects, the overall SNR indicates that thinner slices will be readily obtainable once the protocol and hardware are further optimized. The fact that the HDO concentration in the brain remains below that of body water enrichment at 3 hours indicates that influx of HDO produced outside the brain is not as rapid as might be expected. This is confirmed by the HDO appearance at the longer time points (Figure 2), which does not appear to be approaching a limit even at 3 hours. Additionally, the perdeuterated glucose will not be fully consumed to produce HDO, because glucose is readily distributed throughout the body. For example, in the liver, it could be stored in the form of glycogen,[14] or it could participate in lipogenesis. Both of these processes would limit the total amount of HDO eliminated from [$^2H_7$]glucose given by intravenous injection. A significant consideration for this method is the physiological effect of administering what is equivalent to a glucose tolerance test to the subject.[24] Insulin sensitivity might play a large role in the interpretation of metabolic images produced by this method.

Metabolic imaging of the brain has been a research target driven by both pathophysiological considerations, like stroke and cancer, and by studies of brain structure and cognition as a basic science. Glucose is the primary source of energy in the brain, but the dynamic response of glucose use remains topical. In cancer, aerobic glycolysis is a common metabolic phenotype of many brain malignancies. This change in metabolic programming, often termed Warburg metabolism,[25] is effectively targeted using FDG-PET, which measures excessive glucose uptake but does not otherwise interrogate downstream glucose metabolism. The FDG-PET method has been used to study glucose metabolism in the brain for 40 years[26,27] and has been used to measure functional responses to stimuli.[12] However, total radiation burden makes PET unsuitable in pediatric populations and prevents its serial use in patients.[28] In cognitive psychology, tremendous effort has been expended to map the effects of brain activation using the BOLD methodology (functional MRI).[29,30] Similar techniques measuring cerebral metabolic rate of O_2 consumption (CMRO2) have been used to estimate glucose oxidation as well.[31] All of these methods indirectly infer glucose metabolism without measuring the downstream metabolites. Hyperpolarized ^{13}C does offer the ability to directly detect lactate concentrations and lactate dehydrogenase flux when using hyperpolarized pyruvate as the tracer,[3,6] but this technique demands a special prepolarizer to produce the imaging agent. Furthermore, hyperpolarized glucose is obviously an analogous method, but the short carbon-13 T_1 of glucose makes it difficult to translate to human studies.[6] In contrast, imaging of deuterated agents requires only the addition of a detection coil tuned to the appropriate frequency, and therefore could be easily disseminated to clinical sites. We show here that by imaging HDO, an end product of [$^2H_7$]glucose metabolism, we can produce an image of glucose disposal. This modality should be complimentary to ^{1}H-based methods, and kinetic analysis should yield absolute rates of glycolysis and TCA cycle turnover in healthy tissues.

5 | CONCLUSIONS

We demonstrate here for the first time metabolic imaging of HDO as a biomarker of [$^2H_7$]glucose, lactate, and glx metabolism. Spectrally selective imaging of HDO and glucose using a two-point Dixon method was accomplished with a simple MGE sequence. This modality facilitates higher in-plane resolution and faster acquisition of imaging data than possible with CSI methods.

ACKNOWLEDGMENT

This work was performed at the National High Magnetic Field Laboratory, which is supported by the National Science Foundation (Cooperative Agreement No. DMR-1644779), the State of Florida, and National Institutes of Health (NIH) P41-122698, R01-DK105346, and 5U2C-DK119889. The authors thank Malathy Elumalai and Joshua Slade for construction of the imaging coils and 3D printing of the water phantom container. They also thank Dr. James Bankson for help with the image reconstruction.

ORCID

Rohit Mahar https://orcid.org/0000-0002-9801-4173
Mukundan Ragavan https://orcid.org/0000-0001-8678-4229
Matthew E. Merritt https://orcid.org/0000-0003-4617-9651

REFERENCES

1. Frahm J, Merboldt KD, Hänicke W, Haase A. Stimulated echo imaging. *J Magn Reson (1969)*. 1985;64:81-93.
2. Bottomley PA. Spatial localization in NMR spectroscopy in vivo. *Ann NY Acad Sci*. 1987;508:333-348.
3. Merritt ME, Harrison C, Storey C, Jeffrey FM, Sherry AD, Malloy CR. Hyperpolarized 13C allows a direct measure of flux through a single enzyme-catalyzed step by NMR. *Proc Natl Acad Sci USA*. 2007;104:19773-19777.
4. Salamanca-Cardona L, Keshari KR. 13C-labeled biochemical probes for the study of cancer metabolism with dynamic nuclear polarization-enhanced magnetic resonance imaging. *Cancer Metab*. 2015;3:9.
5. Comment A, Merritt ME. Hyperpolarized magnetic resonance as a sensitive detector of metabolic function. *Biochemistry*. 2014;53:7333-7357.
6. Kurhanewicz J, Vigneron DB, Ardenkjaer-Larsen JH, et al. Hyperpolarized 13C MRI: path to clinical translation in oncology. *Neoplasia*. 2019;21:1-16.
7. Kelloff GJ, Hoffman JM, Johnson B, et al. Progress and promise of FDG-PET imaging for cancer patient management and oncologic drug development. *Clin Cancer Res*. 2005;11:2785-2808.
8. Shreve PD, Anzai Y, Wahl RL. Pitfalls in oncologic diagnosis with FDG PET imaging: physiologic and benign variants. *Radiographics*. 1999;19:61-77; quiz 150-151.
9. Lu M, Zhu X-H, Zhang Y, Mateescu G, Chen W. Quantitative assessment of brain glucose metabolic rates using in vivo deuterium magnetic resonance spectroscopy. *J Cereb Blood Flow Metab*. 2017;37:3518-3530.
10. De Feyter HM, Behar KL, Corbin ZA, et al. Deuterium metabolic imaging (DMI) for MRI-based 3D mapping of metabolism in vivo. *Sci Adv*. 2018;4:eaat7314.
11. Mahar R, Donabedian PL, Merritt ME. HDO production from [2H7]glucose quantitatively identifies Warburg metabolism. *Sci Rep*. 2020;10:8885.
12. Vlassenko AG, Rundle MM, Mintun MA. Human brain glucose metabolism may evolve during activation: findings from a modified FDG PET paradigm. *Neuroimage*. 2006;33:1036-1041.
13. Ragan DK, Bankson JA. Two-point Dixon technique provides robust fat suppression for multi-mouse imaging. *J Magn Reson Imaging*. 2010;31:510-514.
14. De Feyter HM, Behar KL, Corbin ZA, et al. Deuterium metabolic imaging (DMI) for MRI-based 3D mapping of metabolism in vivo. *Sci Adv*. 2018;4:eaat7314.
15. Kreis F, Wright AJ, Hesse F, Fala M, Hu D, Brindle KM. Measuring tumor glycolytic flux in vivo by using fast deuterium MRI. *Radiology*. 2020;294:289-296.
16. Browning JD, Burgess SC. Use of ^2H_2O for estimating rates of gluconeogenesis: determination and correction of error due to transaldolase exchange. *Am J Physiol Endocrinol Metab*. 2012;303:E1304-E1312.
17. Leadlay PF, Albery WJ, Knowles JR. Energetics of triosephosphate isomerase: deuterium isotope effects in the enzyme-catalyzed reaction. *Biochemistry*. 1976;15:5617-5620.
18. Funk AM, Wen X, Hever T, et al. Effects of deuteration on transamination and oxidation of hyperpolarized 13C-pyruvate in the isolated heart. *J Magn Reson*. 2019;301:102-108.
19. Chandramouli V, Ekberg K, Schumann WC, Wahren J, Landau BR. Origins of the hydrogen bound to carbon 1 of glucose in fasting: significance in gluconeogenesis quantitation. *Am J Physiol Endocrinol Metab*. 1999;277:E717-E723.
20. Ben-Yoseph O, Kingsley PB, Ross BD. Metabolic loss of deuterium from isotopically labeled glucose. *Magn Reson Med*. 1994;32:405-409.
21. de Graaf RA, Thomas MA, Behar KL, De Feyter HM. Characterization of kinetic isotope effects and label loss in deuterium-based isotopic labeling studies. *ACS Chem Neurosci*. 2021;12:234–243.
22. Ma J. Dixon techniques for water and fat imaging. *J Magn Reson Imaging*. 2008;28:543-558.
23. Wang Y, Li D, Haacke EM, Brown JJ. A three-point Dixon method for water and fat separation using 2D and 3D gradient-echo techniques. *J Magn Reson Imaging*. 1998;8:703-710.
24. Riis-Vestergaard MJ, Laustsen C, Mariager CØ, Schulte RF, Pedersen SB, Richelsen B. Glucose metabolism in brown adipose tissue determined by deuterium metabolic imaging in rats. *Int J Obes*. 2020;44:1417-1427.
25. Warburg O. On the origin of cancer cells. *Science*. 1956;123:309-314.
26. Phelps ME, Huang SC, Hoffman EJ, Selin C, Sokoloff L, Kuhl DE. Tomographic measurement of local cerebral glucose metabolic rate in humans with (F-18)2-fluoro-2-deoxy-D-glucose: validation of method. *Ann Neurol*. 1979;6:371-388.
27. Villien M, Wey H-Y, Mandeville JB, et al. Dynamic functional imaging of brain glucose utilization using fPET-FDG. *Neuroimage*. 2014;100:192-199.
28. Chawla SC, Federman N, Zhang DI, et al. Estimated cumulative radiation dose from PET/CT in children with malignancies: a 5-year retrospective review. *Pediatr Radiol*. 2010;40:681-686.
29. Yamada H, Sadato N, Konishi Y, et al. A rapid brain metabolic change in infants detected by fMRI. *NeuroReport*. 1997;8:3775-3778.
30. Uğurbil K, Adriany G, Andersen P, et al. Magnetic resonance studies of brain function and neurochemistry. *Annu Rev Biomed Eng*. 2000;2:633-660.
31. Rodgers ZB, Detre JA, Wehrli FW. MRI-based methods for quantification of the cerebral metabolic rate of oxygen. *J Cereb Blood Flow Metab*. 2016;36:1165-1185.

SUPPORTING INFORMATION

Additional Supporting Information may be found online in the Supporting Information section.

FIGURE S1 Correlation plot between [$^2H_7$]glucose consumption and deuterated water (HDO) production. The delivery of [$^2H_7$]glucose into the rat brain peaks at about 850 units of glucose consumption, corresponding to approximately 10 minutes following infusion. [$^2H_7$]glucose consumption is linear with HDO production from 10 to 24 minutes (first dotted line). The second dotted line shows that HDO appearance in the brain remains linear after this first window, but the slope changes as HDO produced by peripheral metabolism begins to arrive in the volume observed by the surface coil

FIGURE S2 Theoretical pyruvate methyl isotopomers generated from [$^2H_7$]glucose, accounting for the singly deuterated pyruvate generated from the C1 position and the doubly deuterated pyruvate generated from the C6 position. The action of ALT can deplete pyruvate of ^2H atoms as well, which is denoted by ALT on/off. Data plotted in Figure 2C was normalized for the exchange mediated loss of deuterium in excess of this statistical prediction using the experimentally determined values of de Graaf (1)

How to cite this article: Mahar R, Zeng H, Giacalone A, Ragavan M, Mareci TH, Merritt ME. Deuterated water imaging of the rat brain following metabolism of [$^2H_7$]glucose. *Magn Reson Med*. 2021;85:3049–3059. https://doi.org/10.1002/mrm.28700